CERN – SL DIVISION

CERN-SL-99-008 HRF

Signatures of microwave instability

E. Shaposhnikova

Abstract

The microwave instability is probably one of the most well known manifestations of collective effects in accelerators. However the theory describing this instability for bunched beams is still under development. The result of the instability is a significant increase in longitudinal emittance of the beam, leading to a serious performance limitation in many machines. In this lecture we first discuss what is the phenomenon that one calls the microwave instability and then describe measurements of instability threshold, momentum spread and spectrum of the unstable bunch.

Lecture given at Joint US-CERN-Japan-Russia Accelerator School on
Beam measurement, Montreux and CERN, Switzerland, 11-20 May 1998

Geneva, Switzerland

25 February 1999

Contents

1 Introduction, or what does one call the microwave instability?

With increasing beam current, in the late 70's, so called turbulent bunch lengthening was observed first in electron and then in proton accelerators: ACO (Orsay, France), ADONE (Frascati, Italy), CEA (Cambridge, USA), SPEAR (SLAC, USA), ISR, PS and SPS (CERN, Switzerland), Main Ring (Fermilab, USA) and in many others.

From the start observations showed that this is a single-bunch phenomenon. Momentum blow-up depended strongly on the intensity per bunch but not on the number of bunches in the ring. The instability also was identified as being in the longitudinal plane of particle motion.

Most probably, the name microwave (μw) instability was first introduced by D. Boussard in 1975 to describe the very large momentum blow-up suffered by proton bunches during debunching in the CERN PS seen together with microwave (above 1 GHz) signals [1]. The model suggested in [1] to explain this single bunch instability used modified coasting beam theory [2]. Later on the name μw instability was also extended to coasting beams to describe, in both longitudinal and transverse planes, instabilities other than the resistive wall and the negative mass. However in this case the frequencies under consideration are very often much below the GHz range.

Usually (but not always) an instability is called the μw instability if the wavelength of the wake field responsible is much shorter than the bunch length. This can be written as

$$\tau f_r \gg 1, \tag{1}$$

where τ is the bunch length in seconds and f_r is the frequency of the impedance which drives this instability. For a coasting beam, condition (1) then means many wavelengths along the ring and frequencies much higher than the revolution frequency – for large rings this can be in the kHz range. For the latest generation of electron storage rings with bunch lengths as small as tens of picoseconds inequality (1) would require the frequency of the impedance to be above 100 GHz. Then again the name μw instability is often used for an instability driven by an impedance with a very high frequency, which however does not satisfy condition (1). There is also the single-bunch transverse microwave instability, which more often has the name transverse mode-coupling instability (TMCI) [3]. The name μw instability is even sometimes used for multibunch instabilities driven by a high frequency impedance [4].

Below, when not specially indicated otherwise, we will talk about the longitudinal single-bunch instability.

All that concerns the theory of the microwave instability is still an open subject for studies. So we will concentrate on a phenomenological description rather than on an overview of the many existing theories [5]-[7]. Even then it is not possible to discuss all manifestations of μw instability. Inevitably some interesting phenomena will be missed – like, for example, the saw tooth instability observed with leptons in the SLC Damping Ring [8], [9] or hysteresis in bunch lengthening at the KEK Accumulation Ring [10].

2 Observations of instability

Regardless of the rich variety of phenomena called by the same name, all authors agree on the intensity-dependent emittance blow-up as being the most evident signature of longitudinal μw instability. The first indication of emittance blow-up in a bunched beam is of course the increase in bunch length with intensity.

A typical observation of the effect of the μw instability on the bunch distribution is presented in Fig. 1. A single proton bunch with length $\tau \simeq$5 ns injected into the SPS at 26 GeV was captured by the 100 MHz RF system and left to circulate in the ring for some time. Measurements of the bunch profile were taken at injection and after 1.5 s for two different bunch intensities using a longitudinal wideband pick-up. As one can see the high intensity bunch observed at the later moment has a distribution and length very different from the initial one. The low intensity bunch has practically not suffered.

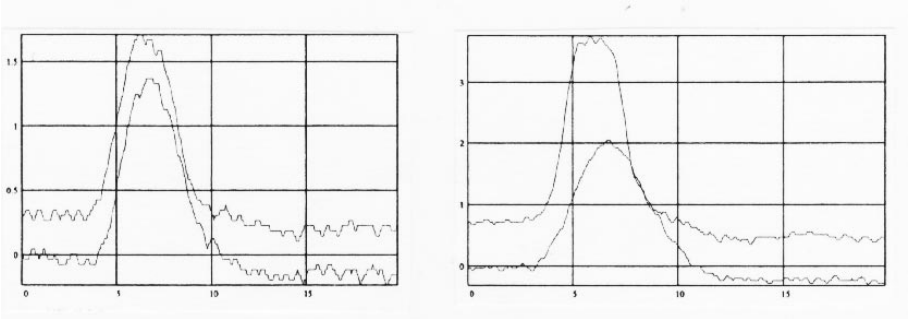

Figure 1: Bunch profile at injection (upper trace) and after 1.5 s (lower trace) for intensity of 2.5×10^{10} (left) and 5.5×10^{10} (right) protons per bunch. Horizontal axis - time (5 ns/div).

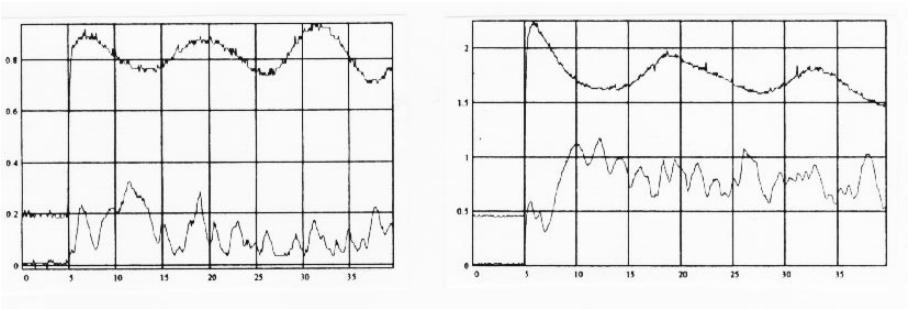

Figure 2: Peak line density (upper trace) and μw signal (lower trace) for intensity of 2.5×10^{10} (left) and 5.5×10^{10} (right) protons per bunch. Horizontal axis - time (5 ms/div).

In Fig. 2 the peak detected signal (peak of line density) observed during the first 35 ms after injection is shown together with the μw signal obtained using a bandpass filter (1.3 - 1.6) GHz for the same bunches as in Fig. 1. The μw signal is significantly larger for the high-intensity bunch (note the change of vertical scale). The differences between the peak detected signals are commented upon later. All data in Figs. 1 and 2 were obtained using the same wideband pick-up.

Measurements of bunch length carried out for different intensities give the bunch lengthening curve. These kinds of curves are obtained in nearly every accelerator in the world. Sometimes this curve has a very clear break-point, as in the classic example from the ISR [11] in Fig. 3 (left), showing two different types of dependence of bunch length on proton intensity. The first part of this curve can be attributed to the change in focusing voltage or synchrotron frequency due to the effect of potential-well distortion. The second part, called in the first observations anomalous or turbulent bunch lengthening, is a signature of the μw instability and the break-point is its threshold.

In the measurements shown in Fig. 1 the intensity was varied in the injector chain. As a result, to analyse the data it is necessary to take into account the possible influence of intensity effects on the bunch shape in the injector itself. This is why in general it is better to change the bunch intensity by vertical scraping at injection or in the transfer line (to keep the longitudinal bunch parameters constant).

It is interesting that the effects of potential-well distortion can already be deduced from the peak detected signal measurements in Fig. 2. Let us assume that the injection voltage (150 kV) is matched so that the incoming "ideal" low-intensity bunch will not have any quadrupole (shape) oscillations after injection. If the voltage is too high then the bunch will start to rotate in longitudinal phase space and become shorter during the first quarter of the synchrotron period. The opposite is true if the voltage is too low – the bunch becomes initially longer. In Fig. 2 the low intensity bunch (on the left) starts to oscillate with an increasing peak line density (upper signal) – for this bunch the voltage is a little bit too high to be matched. The high intensity bunch, on the right, obviously shows that the voltage is too low.

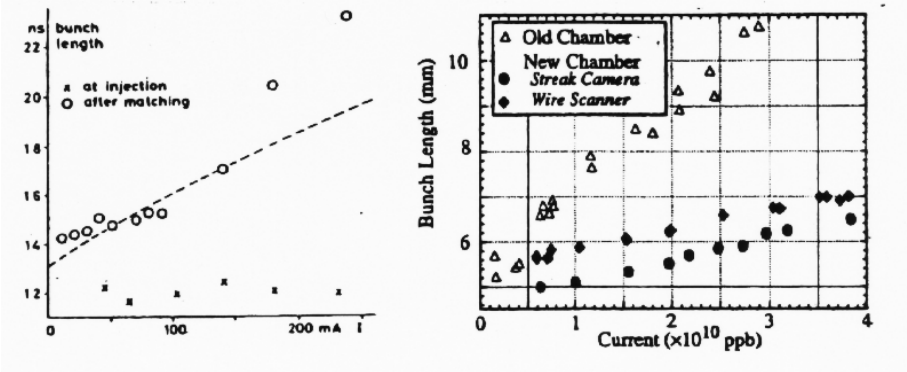

Figure 3: Bunch length as a function of beam current in ISR (left) and in SLC Damping Ring for old and new vacuum chambers (right).

This happens because the potential well provided by the RF system is distorted by the voltage induced even by a stable bunch. If this induced voltage is due to the cavity impedance the effect is called beam loading and usually can be foreseen and compensated in the RF system itself. The voltage induced due to the impedance of other elements in the ring leads to the effect called potential-well distortion. One can also notice in Fig. 2 a reduction in average peak line density during the period of observation – this is already a result of the μw instability.

Very often the bunch-lengthening curve is rather smooth and does not have any clear threshold, as for example in measurements in the SLC Damping Ring presented in Fig. 3 (right) for old and new vacuum chambers [9]. Then one way to distinguish the change in bunch parameters associated with the μw instability from other effects is by measuring the momentum spread (see Fig. 4). Below the instability threshold, if synchrotron radiation effects are important (which usually is true for leptons), momentum spread will stay constant, otherwise (as is true for protons) it is the longitudinal bunch emittance (bunch area in phase space) which is an invariant and momentum spread will change in accordance with bunch length (will decrease if the bunch lengthens).

Some measurement methods of momentum spread, which often plays a key role in identifying the μw instability, are described in the next sections both for bunched and coasting beam.

3 Measurement of momentum spread

In practice there are no direct measurements of beam momentum spread in the machine, however it can be estimated indirectly.

3.1 Bunched beam

3.1.1 From bunch length

For a low-intensity bunch, in the absence of the effect of synchrotron radiation, the most obvious way to estimate momentum spread is to calculate it from the measured bunch length τ for the known synchrotron frequency ω_s. In a non-accelerating bucket, the bunch momentum spread is given by:

$$\frac{\Delta p}{p} = \frac{2\omega_s}{|\eta|\omega_{rf}} \sin\frac{\omega_{rf}\tau}{4}. \tag{2}$$

Here $f_{rf} = \omega_{rf}/(2\pi)$ is the RF frequency, $\eta = 1/\gamma_t^2 - 1/\gamma^2$, where γ and γ_t are the relativistic factors which correspond to the synchronous beam energy E_0 and transition energy.

However, as we have already discussed in the previous section, for a high-intensity bunch the potential-well effect should be taken into account by a voltage modification: $V \rightarrow V + V_{ind}$ and

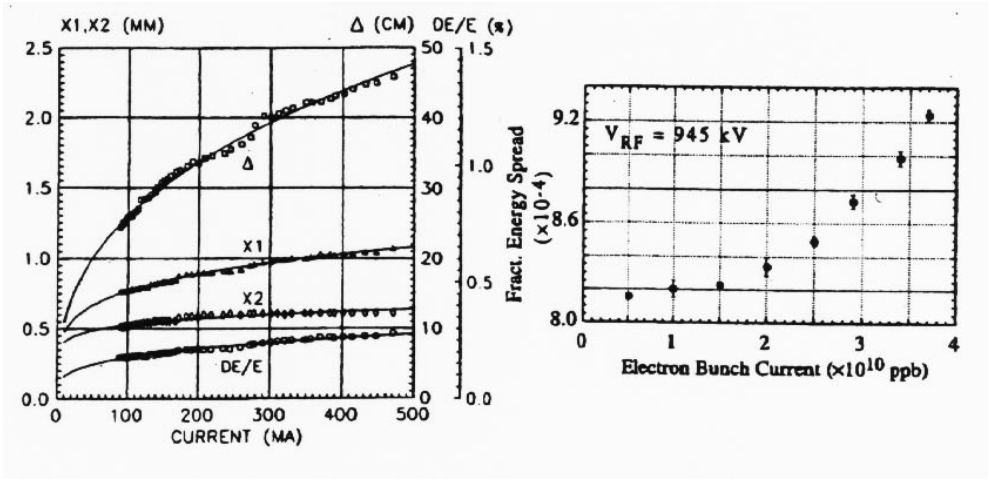

Figure 4: Left: total horizontal size $X1$, betatron size $X2$, energy spread DE/E and bunch length Δ (fwhm) as a function of bunch current in BEP Storage Ring (Novosibirsk). The curves are fits $I_b^{1/3}$ and $I_b^{1/6}$ to the measured data. Right: energy spread measured from transverse beam size in the New SLC Damping Ring.

therefore by replacing $\omega_s^2 \rightarrow \omega_s^2 + \delta$, where δ could be negative or positive. Its sign depends on the machine impedance being inductive or capacitive and the energy E_0 being above or below transition. Space charge below transition has a defocusing effect and leads to bunch lengthening. Bunch shortening due to potential-well distortion is quite rare [12].

3.1.2 From transverse size

Momentum spread can be estimated from the total horizontal beam size

$$\sigma_x^2 = \sigma_\beta^2 + (D_x \frac{\Delta p}{p})^2, \tag{3}$$

where σ_β is the betatron horizontal size and D_x is the dispersion function.

By comparing σ_x measured at the two locations with different D_x one can obtain $\Delta p/p$. To minimise measurement error locations are usually chosen in such a way that D_x is maximum at one and close to zero at the other.

The horizontal beam size can be measured using optical systems (as in LEP, BEP), a wire scanner (SLC Damping Ring, SPS) or others.

In Fig. 4 (left) we present measurements from the BEP Storage Ring (Novosibirsk) [13] done with a resolution ≤ 0.25 mm in the transverse plane and ≤ 2 cm in the longitudinal using an optical diagnostic system. The bunch length follows the $I_b^{1/3}$ curve while energy spread the $I_b^{1/6}$ curve, I_b is the beam current. These measurements allow the intensity dependent increase in bunch length to be explained by the effect of potential-well distortion. The momentum spread increase is a result of multiple intrabeam scattering and not of instability.

The energy spread estimated from the transverse beam size measured in the New SLC Damping Ring [9] with a wire scanner in a dispersive region of the extraction line is shown in Fig. 4 (right). One can clearly see the onset of the instability which was hidden in the corresponding bunch-length measurements presented in Fig. 3.

3.1.3 From debunching

Momentum spread can also be estimated from the speed of debunching. If a bunch is injected into the machine without RF voltage, or if this voltage was switched off, particles which have more or less momentum than the synchronous particle will start to move in different directions and the bunch will become longer.

The initial momentum spread $\Delta p/p$ can be estimated from the decay of the peak detected signal or from the low-frequency bunch spectrum (in the last case assuming that the initial density distribution is known). The low-frequency bunch spectrum during debunching changes with time according to the following expression (up to the instability threshold):

$$S(t,n) = S(0,n^*) \quad n^* = n^*(n,t) = nq(t), \tag{4}$$

where $S(t,n)$ is the signal on the spectrum analyzer at frequency $n\omega_0$, $\omega_0/i(2\pi)$ is the revolution frequency, and $S(0,n)$ is the initial bunch spectrum.

For a short bunch $q(t) = \sqrt{1 + t^2/t_d^2}$ and

$$t_d = \tau_0/(2|\eta|\frac{\Delta p}{p}) \tag{5}$$

is the so called debunching time, τ_0 being the bunch length at injection. During debunching the local value of momentum spread in the bunch is decreasing. The bunch length and peak line density $\lambda_p(t)$ change as

$$\tau(t) = \tau_0 q(t), \qquad \lambda_p(t) = \lambda_p(0)/q(t). \tag{6}$$

In many proton machines the μw instability was observed during RF gymnastics involving debunching. Debunching is also used as a tool in studies of the μw instability [1], [14], [15]. In this way it was understood that local values of momentum spread play an important role.

In Fig. 5 one can see the peak line density decay (peak detected signal) and the μw signal (bandpass filter 1.3 - 1.6 GHz) from a wideband pick-up recorded during debunching of two bunches with different intensities.

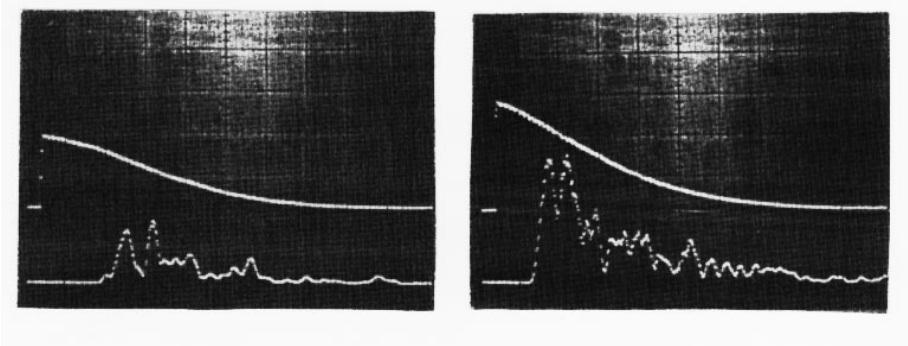

Figure 5: Peak detected (upper trace) and μw (lower trace) signals during debunching of bunches with 3.4×10^{10} (left) and 4.3×10^{10} (right) protons per bunch. Horizontal axis - time (5 ms/div).

Both bunches become unstable during debunching, but the high-intensity bunch at an earlier moment. It is also possible to notice that the high-intensity bunch debunches faster. Below the instability threshold this can be explained by an effect similar to potential-well distortion [16] – in this case the induced voltage has a defocusing effect. During the instability momentum blow-up decreases the debunching time as well, see Eq.(5).

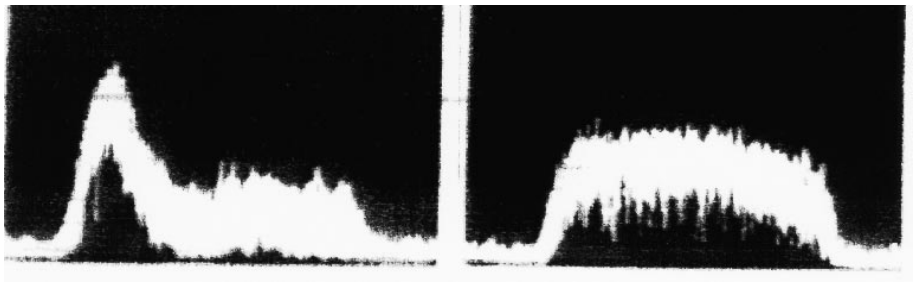

Figure 6: Schottky scan at the beginning (left photo) and at the end (right photo) of debunching in the CERN PS. Horizontal axis - frequency (400 kHz total width), vertical - $\propto \sqrt{F(\omega_0)}$ in logarithmic scale.

3.2 Coasting beam

To confirm the unexpected blow-up in the first studies of the μw instability in the CERN PS [1] momentum spread $\frac{\Delta p}{p}$ was measured at the end of debunching (coasting beam) using different methods. Let us consider some of them.

3.2.1 Shottky scan

In Fig. 6 one can see the increasing width of the Schottky spectrum during debunching (from left to right) due to the effect of the μw instability in the CERN PS [17].

A beam with momentum spread also has a spread in revolution frequencies. The width of the Schottky spectrum $n\Delta\omega_0$ measured at the frequency $n\omega_0$ is related to the momentum spread of the beam by

$$\frac{n\Delta\omega_0}{n\omega_0} = \eta\frac{\Delta p}{p}. \tag{7}$$

The amplitude of the signal at $n\omega_0$ is proportional to the square root of the number of particles at a given revolution frequency.

The frequency $n\omega_0$ should be chosen as a compromise between the width of the line which increases with n as $n\Delta\omega_0$, and the amplitude of the signal which decays with n. For example, for measurements of the Schottky spectrum in the SPS a resonant pick-up with resonant frequency $n\omega_0/(2\pi) = 1$ GHz ($n \sim 23000$) and bandwidth 2 MHz is installed in the ring. This method is based on statistical phenomena and therefore an averaging spectrum analyzer should be used ($\sim$ 100 measurements).

3.2.2 Scanning bucket technique

This technique is based on adiabatically varying the frequency $\omega_{rf}(t)$ to move small empty buckets across the beam in momentum space, (see left picture in Fig. 7). The required frequency variation is

$$\Delta\omega_{rf} > h\Delta\omega_0 = h\eta\omega_0\frac{\Delta p}{p}, \tag{8}$$

where h is the harmonic number. Measurement of the amplitude of the beam spectrum at the frequency ω_{rf} as a function of time during scanning gives the momentum spread. Results for the CERN PS [17] are shown in Fig. 7. While this method was used in many machines at CERN (ISR [18], PS, SPS) it is not straightforward and requires quite fine tuning.

3.2.3 Other methods

For the threshold calculation it is important to know the shape of the particle distribution in momentum. For electrons one usually assumes a Gaussian distribution. For protons the choice is not so obvious.

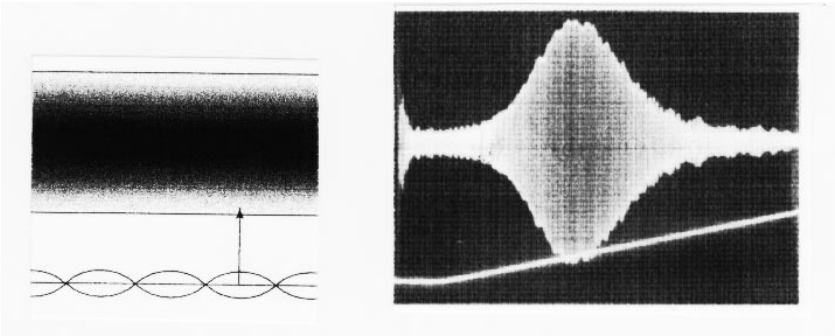

Figure 7: Scanning bucket technique. In the photo measured amplitude of bunch spectrum at ω_{rf} (top signal) together with corresponding change in frequency (lower signal).

Besides those described above there are other methods which allow information about the momentum distribution to be obtained. There are, for example, beam transfer functions (BTF) and beam echos.

The technique for BTF measurements in coasting beam is well developed. Echos in accelerators are quite new. After beam excitation by two short consecutive RF pulses with delay Δt at different harmonics of the revolution frequency h_1 and h_2 an echo signal can be observed at harmonic $(h_2 - h_1)$ and at a time $t_{echo} = h_2\Delta t/(h_2 - h_1)$ after the first kick. The shape of the echo signal in time is proportional to the Fourier transform of the momentum distribution [19].

Disadvantages of these methods are that they are destructive (one needs a kick which can change a distribution) and not intensity independent. But as a result of this intensity dependence the BTF measurement can be used to determine the machine impedance.

4 What is the μw instability?

In the introduction we discussed what is the phenomenon that one calls the μw instability. However it is much more difficult to answer the question what is the μw instability.

The mechanism of the instability is based on the self-action of particles (feedback) which leads to the fact that an initial small density perturbation grows exponentially with time. The action of one particle on the other in the accelerator can be described by the wake field or coupling impedance.

The coupling impedance $Z(\omega)$ is the Fourier transform of the wake potential, proportional to the electric field integrated over one turn as seen by a probe particle following a source particle at a time interval t. An accurate and detailed definition can be found for example in [7], [20], see also these proceedings [21].

A complete picture requires knowledge of both the source of the instability – the coupling impedance, and the mechanism of the self-action — the theoretical model.

Coupling impedance is determined by the beam environment and can be very different in different accelerators.

Usually in old machines the many changes in cross section contribute to a relatively large impedance which is difficult to evaluate. As a result, an impedance model which is a broad-band resonator of the form

$$Z(\omega) = \frac{R_{sh}}{1 + iQ(\omega/\omega_r - \omega_r/\omega)}, \tag{9}$$

with quality factor $Q \simeq 1$ and resonant frequency $\omega_r = \omega_0 n_r$ chosen around the vacuum chamber cut-off, is often assumed. Here R_{sh} is the shunt impedance and the resonator bandwidth is $\Delta\omega_r = \Delta\omega_{hhhw} = \omega_r/2Q$. For bunch lengths which satisfy condition (1), the spectrum of the stable bunch sees a low-frequency impedance $Z/n = iR_{sh}/(Qn_r)$, where $n = \omega/\omega_0$, which together with the space charge effect is responsible for the potential-well distortion discussed above.

Examples of $|Z/n|$ (Ohm) for different accelerators are: CERN ISR - 14, Fermilab MR - 5, Super-ACO - 2.2, LEP - 0.5, ALS - 0.2.

As one can see, in modern accelerators the impedance is smaller and usually better known. A more realistic broad-band impedance model (for example in [22]) is constructed using impedance calculations (in most cases numerical) for different machine elements. Difficulties in this case can arise from the fact that short bunches sample the impedance at very high frequencies, well beyond cut-off.

If the machine coupling impedance is well known then multiparticle simulation codes can be used to try to reproduce the measurement results for the instability. Usually this is done for the bunch-lengthening curve.

The theory of the μw instability for a coasting beam is well understood [2], [23]. First theories analysing bunched beam instabilities were suggested in [24], [25]. It was also proposed [1] that one can apply coasting beam theory to the local parameters in a bunched beam assuming

- fast instability (growth time shorter than synchrotron period),
- wavelength involved $\ll$ bunch length; this is condition (1),
- wake function is a short range (low Q impedance).

This gives the Keil-Schnell-Boussard criterion [1], [23] for the threshold of the longitudinal μw instability, which can be written in the form:

$$\frac{|Z|/n}{F^\star} \leq \frac{pc\beta|\eta|}{e^2 N}(\frac{\Delta p}{p})^2\tau, \tag{10}$$

where N is the number of particles in the bunch and $F^\star$ is a form factor taking into account different particle distributions.

This empirical rule is widely used for impedance estimations and parameter scaling. The observed discrepancy for short bunches [6] can be partially improved by using instead of the low frequency limit Z/n, an effective impedance which is the actual impedance integrated over the bunch spectrum.

For example, threshold measurements done in the CERN SPS during the last 20 years with different beams (protons and leptons) and by different people produced estimations for the impedance $|Z|/n$ (using formula (10)) in the range 9 to 37 Ohm. In all these measurements the bunch length was quite similar – (3 - 5 ns). For much shorter lepton bunches formula (10) predicts an instability threshold which was exceeded in operation many times without any instability being observed [26]. Replacing $|Z|/n$ found for long electron bunches by an effective impedance improves the situation but is still insufficient.

A proof for this criterion has so far been provided [27] for a broad-band impedance with Z/n constant over some bandwidth, much larger than the bunch spectrum width $\propto 1/\tau$. This criterion is also shown [4] to work for a multibunch instability driven by a high-frequency resonator of form (9).

In the next section we will consider measurement of the bunch spectrum. We will show that the spectrum of the unstable bunch contains important information about the source and mechanism of instability. We will distinguish between measurements done close to the threshold and those done well above the instability threshold as being cases of slow and fast instability.

In the case of the fast instability one can assume that bunch behaviour is determined by the induced voltage and that synchrotron motion can be neglected. For fast-decaying wake fields there is no feedback between head and tail of the bunch. For the slow instability synchrotron motion plays an important role – this is how information passes from the tail to the head of the bunch.

5 Bunch spectrum

5.1 Slow instability

The longitudinal motion of the particle can be described by a pair of conjugate coordinates $(\theta, \dot{\theta})$, where θ is an azimuthal position measured relative to the synchronous particle and $\dot{\theta}$ is connected with the

momentum deviation by

$$\dot{\theta} = \omega_0 \eta \frac{\Delta p}{p}. \tag{11}$$

The synchronous particle gives, at the position of the pick-up, a signal with a spectrum of equal amplitude lines at all revolution harmonics $n\omega_0$, $-\infty < n < \infty$.

Let us consider a particle which performs linear synchrotron oscillations described by the phase equation

$$\ddot{\theta} + \omega_s^2 \theta = 0. \tag{12}$$

The amplitude r and phase ψ of these oscillations are:

$$\theta = r \cos \psi, \qquad \dot{\theta}/\omega_s = r \sin \psi.$$

The spectrum of the signal becomes more complicated and has, in addition, synchrotron sidebands around every revolution frequency line at $\omega = n\omega_0 + m\omega_s$, $-\infty < m < \infty$. Their amplitudes are $J_m(nr)$, where $J_m(x)$ is the Bessel function of order m.

In polar coordinates (r, ψ) the evolution of the particle distribution $F(r, \psi, t)$ in longitudinal phase space is described by the Vlasov equation:

$$\frac{\partial F}{\partial t} + \frac{\partial F}{\partial \psi}\omega_s + \frac{\partial F}{\partial r}\dot{r} = 0. \tag{13}$$

Without wake fields $\dot{r} = 0$ and the stationary distribution function is a function of r only: $F = F_0(r)$. The spectrum of the bunch does not show any internal motion and consists of revolution lines with an envelope which is the Fourier transform of the bunch line density $\lambda(\theta)$.

Due to induced voltage V_{ind} the particle motion is perturbed:

$$\ddot{\theta} = \frac{\omega^2 \eta}{\beta^2 E_0} \frac{e}{2\pi} [V_{rf}(\theta) + V_{ind}(\theta, t)]. \tag{14}$$

The distribution function can be decomposed into an equilibrium and a perturbed part:

$$F(r, \psi, t) = F_0(r) + f(r, \psi, t). \tag{15}$$

For small $f(r, \psi, t)$ the Vlasov equation (13) can be linearized and the solution for the perturbation can be written as an expansion in eigenmodes

$$f(r, \psi, t) = \sum_{m=-\infty}^{\infty} \sum_{k=0}^{\infty} a_{mk} R_{mk}(r) e^{im\psi} e^{-i\Omega_{mk} t}, \tag{16}$$

where m and k are the azimuthal and radial mode numbers. In general solutions can only be found numerically. However for some special types of distribution $F_0(r)$ and coupling impedance $Z(\omega)$, there are analytical solutions as well. For more information see [5], [7], [25].

As an illustration, a few examples of bunch line density perturbation creating coherent signals corresponding to different low intensity bunch modes, are shown schematically in Fig. 8, [25], [28]. The perturbation with $m = 1$ and $k = 1$ can be created if a bunch with an excess of particles in some local place in phase space is displaced from the origin as a whole.

Often, instead of k, radial modes are classified by $q = m + 2k$ – the number of nodes which the line density perturbation has inside the bunch [5]. In our example in Fig. 8 the perturbations have the same number of nodes and therefore the same mode number $q = 3$, but different oscillation frequencies and azimuthal mode numbers – $m = 1$ and $m = 3$. The spectrum of these modes consists of sidebands at each revolution line n: $\omega_{nm} = n\omega_0 + m\omega_s$. For the sinusoidal perturbation drawn in Fig. 8 the envelope is maximum at $\omega \sim \pi(q + 1)/\tau$ and extends to $\pm 2\pi/\tau$. Due to the nonlinearity of the external RF field,

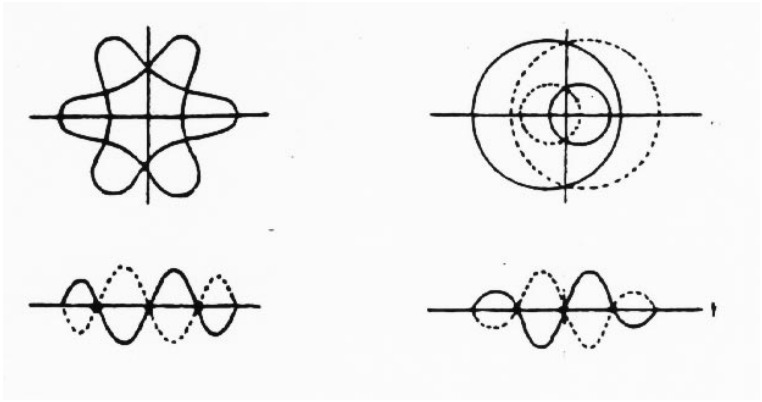

Figure 8: Mode of oscillation with $m = 3$, $k = 0$ (left) and $m = 1$, $k = 1$ (right) in longitudinal phase space (top) and time domain (bottom).

the real spectrum also contains higher harmonics of the synchrotron sideband $m\omega_s$. As one can see identifying radial modes in measurements may not be so obvious. Direct observation of signals in time domain together with spectrum measurements can help to distinguish the different oscillation modes.

At low intensities bunch oscillations with different azimuthal numbers can be considered independently. The coherent frequencies of the oscillations can be found from solving the eigenvalue problem for the following equation derived from the Vlasov equation [25]

$$(\Omega - m\omega_s)a_{mk} = \sum_k M^m_{kk'} a_{mk'}, \tag{17}$$

where M is an interaction matrix with elements

$$M^m_{kk'} = imK \sum_{n=-\infty}^{\infty} \frac{Z(\omega')}{\omega'} g_{mk}(\omega') g_{mk'}(\omega'). \tag{18}$$

Here $\omega' = n\omega_0 + m\omega_s$ and $K \propto N$ is an intensity parameter. For a Gaussian distribution with standard deviation in the bunch length σ_t, the bunch spectrum functions $g_{mn}(\omega)$ are

$$g_{mn}(\omega) = \frac{1}{\sigma_t \sqrt{2\pi k!(m+k)!}} x^{m+2k} e^{-x^2}, \tag{19}$$

where $x = \omega\sigma_t/\sqrt{2}$. These functions peak at the frequency

$$\omega^{max}_{m,k} = \sqrt{m+2k}/\sigma_t. \tag{20}$$

As we discussed above, it is defined only by the value of $q = m + 2k$ (the number of nodes in the bunch signal). The amplitudes of spectrum functions having a maximum at the same position (the same q) are larger for those with lower azimuthal modes m but higher radial modes k.

When the frequency shifts are small compared to ω_s, (and ignoring potential-well distortion), instability is possible only for a narrow-band impedance (Robinson type, not discussed here). Mode coupling theory assumes that at higher intensities the frequency shifts of the modes with different m have different signs and become comparable to ω_s. Depending on the type of impedance (inductive or capacitive) the coherent frequency shift can be negative or positive. For example, for a resonant type of impedance, modes with the lowest radial mode $k = 0$ and two different azimuthal numbers m and $m + 1$ such that $\omega^{max}_{m,0} < \omega_r < \omega^{max}_{m+1,0}$, will be shifted in different directions. According to F. Sacherer's original assumption [25] the instability threshold is defined by the intensity at which these modes couple. Note

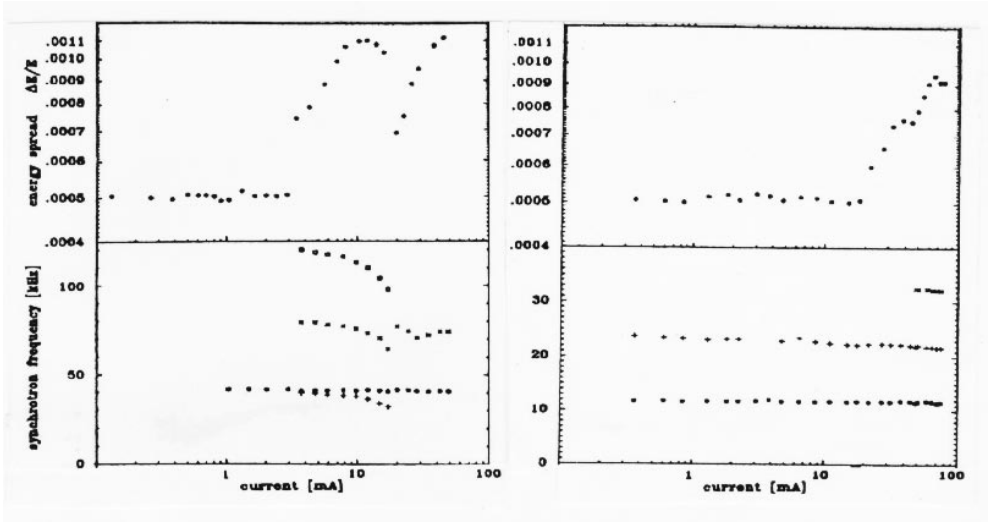

Figure 9: Measurements of energy spread (top) and synchrotron sideband frequencies (bottom) as a function of beam current for two different initial bunch lengths: $\sigma = c\sigma_t$ = 0.854 cm (left) and σ= 3.26 cm (right) in BESSY Storage Ring.

that to drive the instability, an imaginary part of the impedance is not sufficient, one needs the resistive part as well.

Under the assumption that momentum spread and hence bunch length change just enough to stay at the threshold, the intensity parameter K gives the scaling law [29]

$$\tau \propto (\frac{\eta I_{av}\omega_0^2}{E_0\omega_s^2})^{\frac{1}{(2+a)}}, \qquad I_{av} = Ne\omega_0/(2\pi) \tag{21}$$

for the assumed dependence $Z(\omega) \sim \omega^a$. An example is the scaling law for SPEAR [12], where from bunch length measurements the parameter $a = -0.68$ was found.

However coupling between azimuthal modes as a mechanism for the μw instability still waits experimental confirmation in the longitudinal plane. Indeed, motion (m =1) cannot be affected by a self force such as the wakefield gives and therefore the coherent dipole frequency ($m = 1$) does not change with current. The quadrupole frequency (m = 2) does change but usually much less than one needs to explain an instability by mode coupling.

In Fig. 9 we present the results of bunch spectrum measurements in the BESSY Storage Ring [30]. One can see that as bunch intensity increases synchrotron sidebands do shift from their initial value, however the emittance blow-up (see the two graphs at the top) starts much earlier and is more associated with the appearance of higher (m = 2, 3) modes than with their coupling.

Around the threshold of instability one can usually see [6], [12], [30], [31]:

- Growing of higher order modes (usually starting with quadrupole).
- Splitting of modes (radial modes with $k > 0$?).

The method of observing synchrotron sidebands is based on spectrum analysis of a pick-up signal. Good resolution is needed to observe the $m\omega_s$ lines around a revolution frequency line $n\omega_0$ outside the stable bunch spectrum, which extends up to $2\pi/\tau$.

Another measurement of synchrotron sideband behaviour below and above instability threshold, done by K.Satoh [6] is shown in Fig. 10. The instability threshold when the energy spread starts to increase, was found to be at 7 mA. It is clear that the sidebands do not overlap at this intensity. Measurements were taken around the carrier at 4.461 GHz.

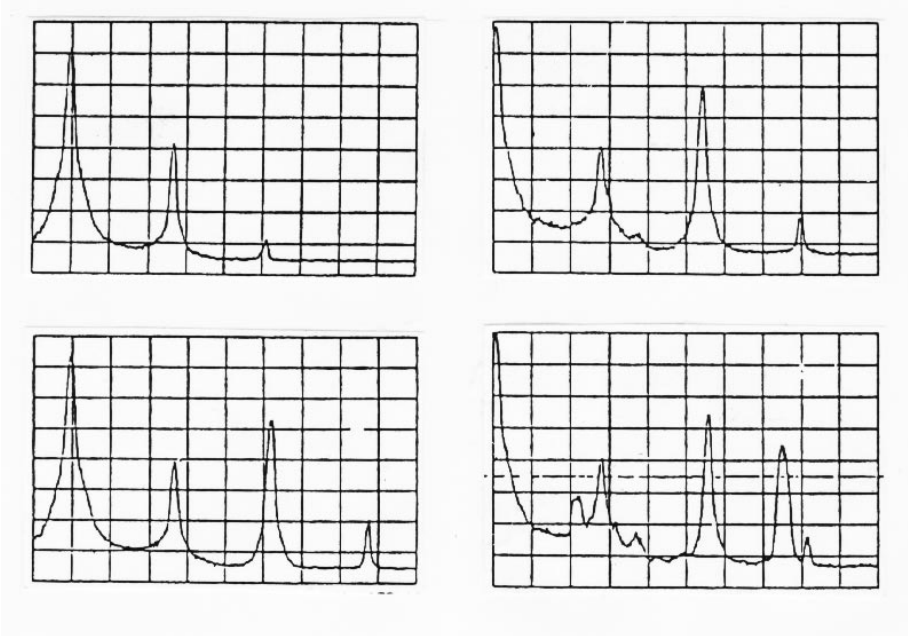

Figure 10: Synchrotron sideband evolution with current measured in TRISTAN-AR for beam current 3.1 mA (top left), 5.2 mA (bottom left), 6.3 mA (top right) and 7.9 mA (bottom right). Span 10 kHz.

In conclusion mode coupling has not been clearly observed in the longitudinal plane. Very often the measured instability threshold coincides with an onset of coherent oscillations. In the analysis based on the Vlasov equation the instability of a single azimuthal bunch mode can be obtained if the effect of potential-well distortion is explicitly taken into account [32] - [35].

It was found quite a long time ago that potential-well distortion may play an important role in instability threshold calculations [24], [36]. Nonlinearity of the wakefield [33] distorts the potential well in such a way that the equilibrium particle distribution becomes a function of phase ψ also. It was shown that in a distorted potential well coupling between radial modes belonging to the same azimuthal mode becomes possible [34]. Degeneration of the synchrotron frequency at two different amplitudes inside the bunch has been suggested as another possible mechanism for the longitudinal single-bunch instability [35].

These effects are most pronounced for a resistive wake and are of second order in bunch intensity N. This may clarify the following experimental fact: in the SLC Damping Ring after the reduction of the machine impedance (which became mostly resistive) the threshold of the instability decreased [9], see Fig. 3 (right). However the subsequent bunch lengthening observed was much smaller.

Sometimes the difficulty of finding a self-consistent solution for the stationary distribution above some intensity is interpreted as the threshold for the instability. However this problem can be of a numerical nature [37].

Unlike the longitudinal μw instability, in the transverse plane mode-coupling theory (TMCI) has been succesfully used to explain the fast single-bunch instability first observed in PETRA [3]. In many electron machines, Super-ACO, EPA, LEP and others, mode coupling was measured and results are in reasonable agreement with theory.

Transverse mode-coupling instability has not been observed in proton machines. An obvious difference is the particle mass and therefore the value of the relativistic factor. Apart from synchrotron radiation, this can be important for space charge effects, when stabilization may come from the incoherent synchrotron frequency spread. Other bunch parameters could be very similar, as for example in the CERN SPS: at 3.5 GeV leptons have a damping time (4.5 s) and a length ($\sigma_t = 1$ ns) similar to proton bunches at 26 GeV. Leptons are unstable both at injection and later in the cycle. Using an impedance

model able to explain all the experimental data for leptons [26], instability is predicted for protons, but was never seen. Note that for long bunches high radial modes ($k > 0$) play an important role in making correct estimations of the TMCI threshold.

5.2 Fast instability

We defined the fast instability as one which develops during a period of time shorter than the synchrotron period. From this we conclude that the mechanism of this instability is different from that discussed in the previous section. The theory of the fast μw instability has been considered in many papers, see for example [27], [38], [39].

If synchrotron motion does not play an important role then the development of the instability should be similar for the two cases, RF on and RF off, if in the last case debunching is slow during the growth of the instability. This fact was used in measurements of the unstable bunch spectrum done in the CERN SPS [40]. These measurements allowed the elements in the ring responsible for the μw instability to be identified. The method of measurement is described in detail in the next section.

Let us start with a simple illustration of the principle. Below the instability threshold the bunch has a spectrum which is concentrated at low frequencies, with width proportional to $1/\tau$. Now let us assume that the bunch line density has some small modulation at a frequency ω_r. Then the spectrum of this bunch will have an additional peak at this frequency as presented in Fig. 11. The width of this peak is again inversely proportional to the bunch length. As will be shown, above the instability threshold the presence of a narrow-band resonant impedance leads to line density modulation and therefore to this type of bunch spectrum.

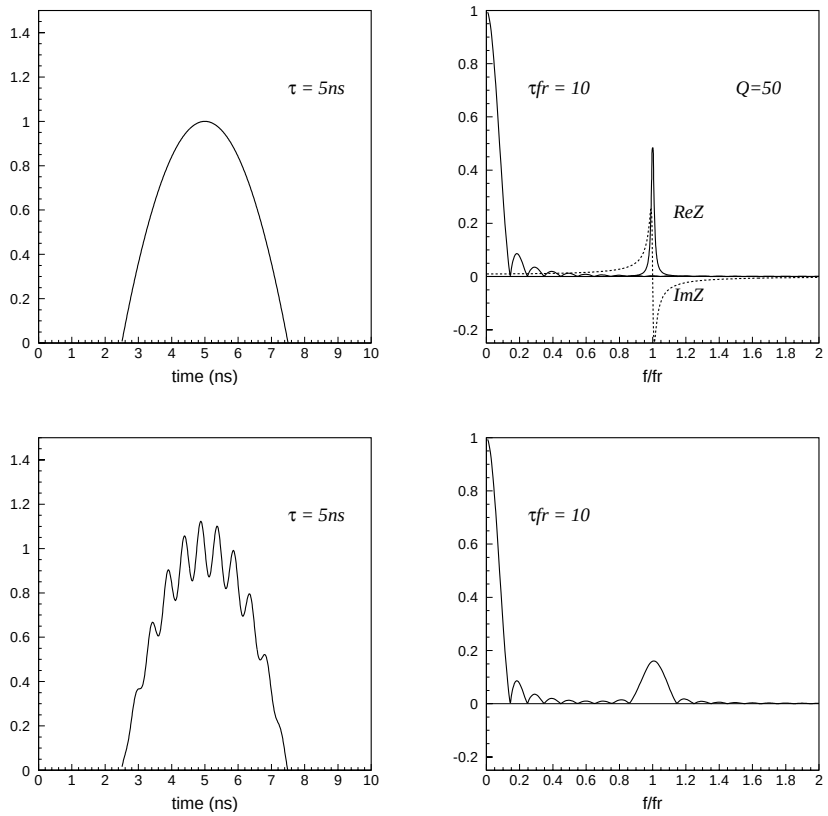

Figure 11: Stable (top) and unstable (bottom) bunches (left) and their spectrum (right).

To analyse the fast instability it is natural to use an expansion of the line density perturbation $\rho(\theta, t)$

in azimuthal harmonics:

$$\rho(\theta,t)=\sum_n \rho_n e^{in\theta}, \tag{22}$$

where

$$\rho_n=\frac{1}{2\pi}e^{-i\Omega t}\int\int f(\theta,\dot{\theta})e^{-in\theta}d\theta d\dot{\theta} \tag{23}$$

and the growth rate of the instability is defined by the imaginary part of the coherent oscillation frequency Ω.

The voltage induced by the beam is

$$V_{ind}=-e\omega_0\sum_n(G_n+\rho_n)Z_n\exp{(in\theta)}. \tag{24}$$

Using the linearised Vlasov equation leads to the same matrix equation as in the analysis of a fast microwave instability in the system with RF on, when the synchrotron motion in fact is neglected [27]. For a monoenergetic bunch with $F(\theta,\dot{\theta})=G(\theta)\delta(\dot{\theta})$, this equation can be written in the form

$$\rho_n=-i\frac{\eta n\omega_0}{2\pi E_0}(\frac{e\omega_0}{\Omega})^2\sum_{n'}G_{n-n'}Z_{n'}\rho_{n'}, \tag{25}$$

where G_n is the Fourier transform of $G(\theta)$.

The exact solution of equation (25) can be found for a coasting beam, where the distribution function does not depend on the azimuthal coordinate θ and therefore

$$G_{n-n'}=N\delta_{n,n'}. \tag{26}$$

In this case the perturbed bunch spectrum consists of signals at the revolution lines with the growth rate which can be calculated from the expression:

$$\Omega_n^2=-i\frac{(en\omega_0)^2N\omega_0}{2\pi E_0}\eta\frac{Z_n}{n}. \tag{27}$$

For a pure imaginary impedance (inductive or capacitive), $Z=i\mathrm{Im}Z$, this formula describes the negative mass instability which can occur if $\eta\mathrm{Im}Z/n<0$.

Now let us consider a single bunch interacting with a resonant impedance, centered at harmonic $n_r=\omega_r/\omega_0$ and with $\omega_r\tau\gg 1$. In this case we can ignore the voltage induced by the unperturbed bunch spectrum. Assume now that the impedance has nonzero value only inside some bandwidth which is much less than the bunch spectrum width $\propto 1/\tau$. Then the bunch spectrum in Eq. (25) can be assumed constant over the impedance width with $G_{n-n'}\simeq G_{n-n_r}$ for $n>0$ and $G_{n-n'}\simeq G_{n+n_r}$ for $n<0$. In this approximation the growth rate does not depend on the harmonic number and can be obtained by summation over n in Eq. (25). For a resonant impedance of form (9) inside the bandwidth and zero outside

$$\frac{\mathrm{Im}\Omega}{\omega_r}\simeq\left(\frac{Ne^2\omega_0|\eta|}{16\pi E_0}\frac{R_{sh}}{Q}\right)^{\frac{1}{2}}. \tag{28}$$

If $\mathrm{Im}\Omega\tau\gg|\eta|\Delta p/p$, the assumption of slow debunching is justified.

The spectrum of the unstable modes is

$$\rho_n\sim nG_{n-n_r}. \tag{29}$$

As we expected it is centered at $n=n_r$ and has a width inversly proportional to the bunch length. The same spectrum is obtained with a narrow-band resistive impedance [41], [42].

By finding the maxima in the unstable bunch spectrum it should be possible to measure the frequency of guilty resonant impedances. It follows from Eq.(28) that one can also hope to determine the R_{sh}/Q by

measuring the growth rate of the bunch spectrum for the unstable mode. However due to the complicated structure of the signal in time, the growth rate is ill-defined in comparison to the maximum value of the mode amplitude, see Fig. 12 (left).

Another approach based on the analysis of the instability in space-time domain [39] shows that the spectrum centered at n_r can be obtained at the initial stages of the instability for a broad-band impedance as well. However in this case its width will be defined by the bandwidth of the impedance. Note that similar results were obtained by the author in multiparticle turn-by-turn simulation.

5.2.1 Measurements in the CERN SPS

Single high-intensity proton bunches were injected into the accelerator with RF off above transition energy at 26 GeV [40]. The maximum amplitude of the signals growing after injection within the first 100 ms was recorded in the frequency range 100 MHz to 4 GHz using a wideband longitudinal pick-up with a spectrum analyser as a receiver (bandwidth 3 MHz), see example in Fig. 12 (left). The data were taken for at least ten different bunches and then averaged. The results are shown in Fig. 12 (right) for relatively short (τ = 4 ns, upper curve) and long (τ = 28 ns - dashed line, τ = 25 ns - solid line) bunches. As expected, see Eq.(29), long bunches give much better resolution. Additional smearing of the peaks comes from the faster debunching of the short bunches. Nevertheless both spectra show common features. Results of measurements with slightly different long bunches are very similar as seen in Fig. 12.

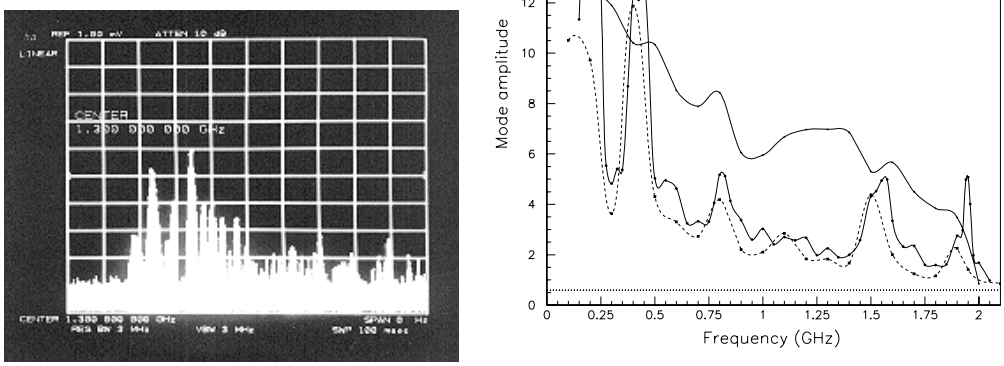

Figure 12: Left: bunch spectrum component at 1.3 GHz for a short bunch as a function of time, 10 ms/div. Right: spectral distribution measured with short (upper curve) and long (lower curves) bunches.

Since the maximum amplitude at a given frequency is recorded, measurements involve the nonlinear stage of the instability, which can be better understood using numerical simulations. These simulations show that the maximum in the bunch spectrum is slightly shifted from the resonant frequency of the impedance (it is higher above transition and lower below transition) and this shift increases with intensity. One can also observe the generation of higher harmonics of the resonant frequency. Therefore care should be taken when interpreting the experimental data.

Another way of observing the bunch spectrum is presented in Fig. 13. This is similar to the illustration in Fig. 11. In Fig. 13 the bunch profile, measured every 100 turns from injection, is presented in the first plot as a mountain range display. The unstable modes grow on the bunch and by taking the Fourier Transform of each profile we see clearly in the second plot the increase of signals with a definite

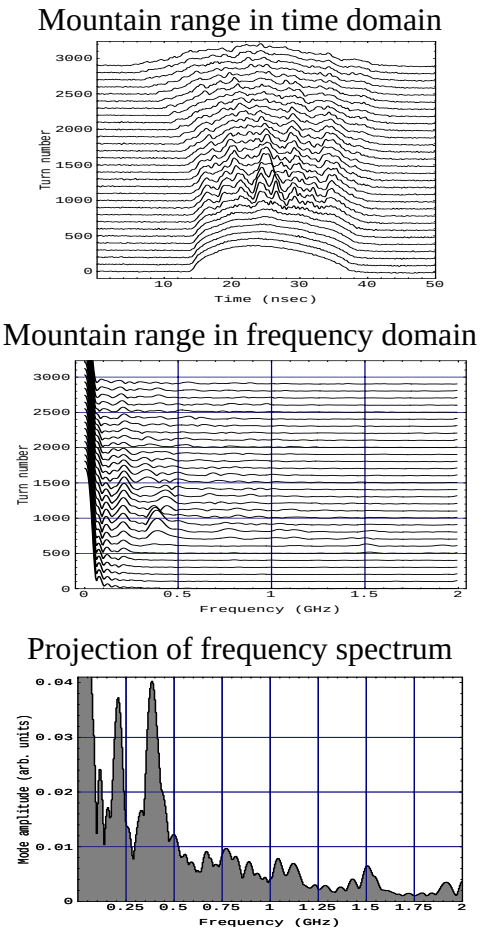

Figure 13: Longitudinal bunch profiles turn by turn and their Fourier analysis.

width at each frequency corresponding to the different impedance sources. Note that a single bunch has already a rich mode structure.

The spectrum produced from shot to shot by bunches with similar parameters can be slightly different, but on average they give reproducible results. The projection of the spectra from Fig. 13 averaged over many bunches would give similar results to Fig. 12 (right). This method was limited to an upper frequency of 2 GHz by the sampling rate of the fast oscilloscope (4 GHz).

The spectrum measured with a spectrum analyser over the frequency range 0.1 to 4.3 GHz is shown in Fig. 14. The injector (PS) was able to provide the following necessary bunch parameters: bunches were long (25 ns) – to have good resolution in the frequency domain, with small momentum spread (2×10^{-4}) – so that they were immediately unstable and their debunching was very slow. The debunching time defined in Eq.(5) is inversely proportional to momentum spread (a monoenergetic bunch would never debunch!). The slow debunching of these bunches can also be seen in Fig. 13 (top).

In this case (SPS) it was possible to decode the signature of the μw instability and determine the impedance sources responsible for it. The peaks at 200 MHz and 800 MHz in Fig. 14 are from the fundamental mode of the two travelling wave RF systems which have high R_{sh}/Q and low Q ($\sim$ 130). Small peaks from 0.4 GHz to 1.4 GHz can be identified with some of the HOM modes of the six SPS RF systems. However the sources of peaks at 400 MHz and above 1.4 GHz were not obvious.

Frequencies above 1.4 GHz suggest cavity-like devices with a radius r_c of around 8 cm. In the SPS there are about 800 pumping ports which fit this criterion and can explain all the high frequency resonances. It is interesting that the simple formula for the resonant frequency for the TM_{mnl} modes of

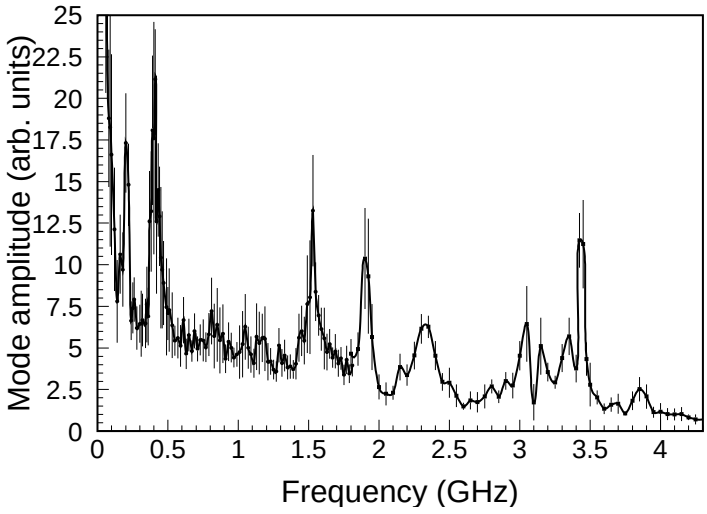

Figure 14: Measured spectral distribution in the range (0.1 - 4.3) GHz.

a cylindrical cavity

$$f_r = \frac{\omega_r}{2\pi} = \frac{c}{2}\sqrt{\left(\frac{l}{z}\right)^2 + \left(\frac{u_{m,n}}{\pi r_c}\right)^2} \tag{30}$$

is in good agreement with the frequencies observed. Here z is the cavity length, l is the axial mode number and $u_{m,n}$ is the n-th root of equation $J_m(u) = 0$. For an axial longitudinal electric field, TM_{0nl} modes, u_{01} = 2.405 and u_{02} = 5.52.

From Eq.(30), for r_c = 8.2 cm and z = 24.0 cm, one can easily find the lowest frequencies of the TM_{01l} and TM_{02l} modes (l = 0,1,2...)

$$1.4, 1.53, 1.88, 2.34, 2.87, 3.2, 3.42, 3.7, 4.0...\text{[GHz]}.$$

They can all be seen in Fig. 14 at close frequencies. The first mode has low $R_{sh}/Q = 3.9$ Ohm (one cavity) and is hardly visible in the spectrum whereas the second has 27.8 Ohm and gives a large peak. These accidental cavities have always been damped by ceramic resistors (laboratory measurements give a $Q \leq 100$), so that they become less dangerous for coupled-bunch instabilities. However damping does not change R_{sh}/Q which is what counts for single-bunch instability, see Eq.(28).

A search for objects with resonant frequencies around 400 MHz led to identification of the magnetic extraction septa (16 tanks in the ring) as the guilty elements.

A programme to reduce the SPS coupling impedance by shielding the vacuum ports and the septum magnets has started. This is important for providing the bunch parameters required when the SPS will become an injector for LHC.

6 Conclusions

- There is a rich variety of phenomena related to the μw instability.
- In general the μw instability is not yet completely undestood and is a hot research topic since it is a serious performance limitation in many accelerators.
- The coasting beam criterion modified for a bunched beam works quite well in many cases, especially for long bunches.

- More observations are required to confirm the mechanism of mode coupling instability in the longitudinal plane.
- The unstable bunch spectrum contains important information about the mechanism and the source of the instability.

As B.Zotter stated at the KEK 1990 ICFA Workshop [6]: “Computer simulation always agrees with theory if done by the same person”.

Measurements are extremely important!

7 Acknowledgments

I am grateful to A. Hofmann and B. Zotter for useful discussions on the contents of this lecture. I would like to thank D. Boussard, A. Chao and T. Linnecar for reading the paper and making helpful comments.

References

[1] D. Boussard, CERN Report LabII/RF/Int./75-2 (1975).

[2] V.K. Neil, A.M. Sessler, Rev. Sci. Instr. **6**, 429 (1965).

[3] R.D. Kohaupt, Proc. 11th Int. Conf. High Energy Acc., Geneva, 562 (1980).

[4] V.I. Balbekov, S.V. Ivanov, Atomnaya Energia, **59**, N1, 42 (1985).

[5] J.L.Laclare, CERN Accelerator School 1985, CERN 87-03, 264 (1987).

[6] Proc. 4th ICFA Beam Dynamics Workshop, Collective Effects in Short Bunches, KEK Report 90-21 (1991).

[7] A. Chao, Physics of Collective Beam Instabilities in High Energy Accelerators, (J. Wiley & Sons, New York, 1993).

[8] P. Krejcik et al., Proc. 1993 IEEE PAC, Washington D.C., 3240 (1993).

[9] K. Bane et al., Proc. 1995 PAC, Dallas, 3109 (1995).

[10] T. Ieiri, Proc. 5th EPAC, 1066 (1996).

[11] S. Hansen et al., IEEE Trans. Nucl. Sci. NS-22, 1381 (1975).

[12] P.B. Wilson et al., IEEE Trans. Nucl. Sci. NS-24, 1211 (1977).

[13] V.V. Danilov et al., Proc. 15th Int. Conf. High Energy Acc., Hamburg, 1115 (1992).

[14] P. Bramham et al., IEEE Trans. Nucl. Sci. NS-24, 1490 (1977).

[15] K.-Y. Ng, Fermilab Report FNAL-TM-1389 (1986).

[16] T. Linnecar, E. Shaposhnikova, Proc. 5th EPAC, 1323 (1996).

[17] D. Boussard, private communication.

[18] W. Schnell, IEEE Trans. Nucl. Sci. NS-20, 747 (1973).

[19] O. Brüning et al., Proc. 5th EPAC, 1332 (1996).

[20] B. Zotter, S. Kheifets, Impedances and Wakes in High Energy Particle Accelerators, (World Scientific, Singapore, 1998).

[21] Y.H.Chin, this course.

[22] S. Bartalucci et al, NIM A **337**, 231 (1994).

[23] E. Keil, W. Schnell, CERN Report ISR-TH-RF/69-48 (1969).

[24] A.N. Lebedev, Atomnaya Energia, **25**, N2, 100 (1968).

[25] F.J. Sacherer, IEEE Trans. Nucl. Sci. NS-24, 1393 (1977).

[26] T. Linnecar, E. Shaposhnikova, CERN Report SL/93-43 (1993).

[27] J.M. Wang, C. Pellegrini, Proc. 11th Int. Conf. High Energy Acc., 554 (1980).

[28] J. Gareyte, CERN Report SL/91-09 (AP), (1991).

[29] A.W. Chao, J. Gareyte, Part. Acc. **25**, 229 (1990).

[30] W. Anders, Proc. 3rd EPAC, 798 (1992).

[31] D. Brandt, K. Cornelis, A. Hofmann, Proc. 3rd EPAC, 345 (1992).

[32] K. Oide, K. Yokoya, KEK Preprint-90-10 (1990).

[33] X.T. Yu, J.S. Wurtele, IEEE Part. Accel. Conf., Washington D.C., 3327 (1993).

[34] A. Chao, B. Chen, K. Oide, Proc. 1995 IEEE PAC, Dallas, 3040 (1995).

[35] K. Oide, KEK Preprint 94-138 (1994).

[36] A. Ruggiero, IEEE Trans. Nucl. Sci. NS-24, 1205 (1977).

[37] Y. Shobuda, K. Hirata, Preprint KEK 98-28 (1998).

[38] M. Month, E. Messerschmid, IEEE Trans. Nucl. Sci. NS-24, 1208 (1977).

[39] A.V. Burov, N.S. Dikansky, D.V. Pestrikov, 13th Int. Conf. High Energy Acc., Novosibirsk, 145 (1986), in Russian.

[40] T. Bohl, T.P.R. Linnecar, E. Shaposhnikova, Phys. Rev. Let., **78**, N16, 3109 (1997).

[41] S. Krinsky, J.M. Wang, IEEE Trans. Nucl. Sci. NS-30, 2494 (1983).

[42] K.Y. Ng, Proc. 1986 Summer Study on Phys. of SSC, 590 (1986).